



OPEN

## Fractional boundary element solution of three-temperature thermoelectric problems

Mohamed Abdelsabour Fahmy<sup>1,2✉</sup>, Mohammed M. Almeahmadi<sup>3</sup>, Fahad M. Al Subhi<sup>1</sup> & Ayesha Sohail<sup>4</sup>

The primary goal of this article is to propose a new fractional boundary element technique for solving nonlinear three-temperature (3T) thermoelectric problems. Analytical solution of the current problem is extremely difficult to obtain. To overcome this difficulty, a new numerical technique must be developed to solve such problem. As a result, we propose a novel fractional boundary element method (BEM) to solve the governing equations of our considered problem. Because of the advantages of the BEM solution, such as the ability to treat problems with complicated geometries that were difficult to solve using previous numerical methods, and the fact that the internal domain does not need to be discretized. As a result, the BEM can be used in a wide variety of thermoelectric applications. The numerical results show the effects of the magnetic field and the graded parameter on thermal stresses. The numerical results also validate the validity and accuracy of the proposed technique.

### Nomenclature

$\beta_{ij}$	Stress–temperature coefficients
$\delta_{ij}$	Kronecker delta ( $i, j = 1, 2$ )
$\varepsilon_{ij}$	Strain tensor
$\varepsilon_{ijk}$	Permutation symbol
$\epsilon_{ij}$	Micro-strain tensor
$\lambda$	Tractions
$\mu_0$	Magnetic permeability
$\pi_0$	Peltier coefficient
$\rho$	Density
$\sigma_{ij}$	Stress tensor
$\sigma_0$	Reference stress
$\sigma_0$	Electric conductivity
$\tau$	Time
$\tau_0, \tau_1, \tau_2$	Relaxation times
$\hat{A}$	Unified parameter
$a$	Fractional order parameter
$B_i$	Magnetic strength components
$c_\alpha$	Specific heat capacities
$C_{ijkl}$	Constant elastic moduli
$E_i$	Electric field vector
$e$	= $\varepsilon_{kk}$ Dilatation
$F_i$	Mass force vector
$\bar{U}_{il}$	Permittivity tensor
$H_i$	Magnetic field intensity
$H_0$	Constant magnetic field
$J_i$	Electric density vector
$\mathbb{K}_\alpha$	Conductive coefficients

<sup>1</sup>Department of Mathematics, Jamoum University College, Umm Al-Qura University, Alshohdaa, Jamoum, Makkah 25371, Saudi Arabia. <sup>2</sup>Faculty of Computers and Informatics, Suez Canal University, New Campus, Ismailia 41522, Egypt. <sup>3</sup>Department of Mathematical Sciences, Faculty of Applied Sciences, Umm Al-Qura University, Makkah 24381, Saudi Arabia. <sup>4</sup>Department of Mathematics, Comsats University Islamabad, Lahore Campus, Lahore 54000, Pakistan. ✉email: maselim@uqu.edu.sa

$k_0$	Seebeck coefficient
$m$	Functionally graded parameter
$P$	Total energy of unit mass
$p$	Pore pressure
$T_\alpha$	Temperature functions
$T_{\alpha 0}$	Reference temperature
$u_i$	Displacement vector
$W_{ei}$	Electron–ion energy coefficient
$W_{er}$	Electron–phonon energy coefficient

Utilizing initial conditions and boundary conditions at  $m$  and Max Planck proposed the quantum theory of electromagnetic radiation in 1900, and Albert Einstein proposed the concept of photons and phonons in 1905 and 1907 to explain why temperature varies with the specific heat of solid crystals. A phonon is a quantum of vibrational mechanical energy produced by a lattice of oscillating atoms, where the thermal energy of the atoms causes the lattice to vibrate. This generates compression mechanical waves, which carry heat and sound through the anisotropic material. The careful study of phonons is an important part of solid-state physics because it is important for many thermal and acoustic properties of solids, as well as a variety of low- and high-temperature superconductive technologies. Many bodies undergo significant changes in their properties as a result of the application of an electric or magnetic field, allowing for the profitable application of this fact in technological applications. The development of electrorheological and magnetic fluids has piqued the interest of many people due to their potential applications in clutches, actuators, shock absorbers, valves, and exercise equipment, to name a few. Field dependent solids, also known as electro-active elastomers, were recently developed by infusing elastomers with electrorheological fluids or embedding them with electrically conducting particles. Magneto-active elastomers, on the other hand, were created by encapsulating elastomers with magnetically responsive particles. Such field dependent solids have potential applications due to the change in structure and the resulting effect on the elasticity and compliance of the material, such field dependent solids have potential applications in a wide range of applications.

Adaptive algorithms based on fractional calculus (FC) have been proposed for parameter estimation of various problems<sup>1,2</sup>, and they outperform standard adaptive methodologies in terms of convergence speed and estimation accuracy<sup>3</sup>. FC is concerned with the calculation of real-order derivatives and integrals<sup>4</sup>. The FC has been successfully used to solve problems in circuit design<sup>5</sup>, artistic paintings<sup>6</sup>, vibration analysis<sup>7</sup>, hydro turbine systems<sup>8</sup>, control engineering<sup>9,10</sup>, nanotechnology<sup>11</sup>, and biological processes<sup>12,13</sup>. Fractional adaptive algorithms are used to estimate the parameters of power signals. The fractional order least mean square (FOLMS) technique is used to estimate the amplitude and phase of power signals<sup>14</sup>. The momentum FOLMS (mFOLMS) was created to speed up the convergence speed of conventional FOLMS<sup>15</sup>. Experiments have shown that the mFOLMS algorithm outperforms the traditional LMS and standard FOLMS algorithms in terms of convergence speed. The FOLMS and mFOLMS performance are unaffected by the fractional order. The so-called innovative FOLMS (I-FOLMS) adaptive algorithm<sup>16</sup>, on the other hand, was recently developed, indicating a strong reliance on fractional order. The I-FOLMS solves the opposing requirements of fast convergence speed and small steady-state error by using an appropriate fractional order selection. The fractional order parameter was discovered to be capable of influencing the initial convergence speed and estimation accuracy of I-FOLMS. These intriguing properties of the I-FOLMS necessitate further research into the I-FOLMS for parameter estimation of power signals, as well as comparisons with the regular FOLMS.

Several studies have investigated the heat transfer in nanofluids<sup>17–19</sup> and magnetohydrodynamic (MHD) flow of nanofluid<sup>20,21</sup>. Nazeer et al.<sup>22</sup> studied the Magnetohydrodynamics (MHD) electro-osmotically flow of third-grade fluid in micro channel. The heat flux on bio-convective flow of Maxwell liquid configured by a stretched nano-material surface was investigated by Chu et al.<sup>23</sup>. Zhao et al.<sup>24</sup> implemented artificial neural networking (ANN) for heat generation in non-Newtonian fluid between two rotating disks. Wang et al.<sup>25</sup> studied the heat transport in non-Newtonian fluid (Oldroyd-B model). Khan et al.<sup>26</sup> studied the heat transport in squeezing nanoliquid flow of non-Newtonian (second-grade). Raja et al.<sup>27</sup> studied the entropy generation in MHD third-grade nanofluid.

Knopoff<sup>28</sup> and Chadwick<sup>29</sup>, followed by Kaliski and Petykiewicz<sup>30</sup>, pioneered the magnetoelasticity foundations. Magnetic theory development and application were previously solely based on magnetic experiments. Because of the rapid development of high-performance computational methods and computer hardware, efficient and accurate computational methods for modeling and simulation of real magnetic experiments have been used, particularly when the magnetic experiment is difficult, dangerous, or expensive.

Fahmy solved magneto-thermo-viscoelastic problems of rotating nonhomogeneous anisotropic solids using the boundar element technique<sup>31–35</sup>. Furthermore, Fahmy used the boundary element method to investigate transient magneto-thermoviscoelastic plane waves in nonhomogeneous anisotropic thick strips<sup>36</sup> and transient micropolar-magneto-thermoelastic plane waves in nonhomogeneous anisotropic structures<sup>37,38</sup>.

The interaction between magnetic and strain fields in a thermoelastic solid is receiving increased attention due to its numerous applications in geophysics, plasma physics, and other fields. All of the articles cited above assumed that interactions between the two fields occur via Lorentz forces appearing in equations of motion and a term entering Ohm's law and representing the electric field created by the velocity of a material particle traveling in a magnetic field. In these investigations, the heat equation under consideration is typically the uncoupled or coupled theory, rather than the generalised one. Ezzat and Awad developed a model of micropolar generalised magneto-thermoelasticity based on modified Ohm's and Fourier's laws<sup>39</sup>. In the literature, several fractional-order models have been investigated for various applications. There is no general analytical solution due to the

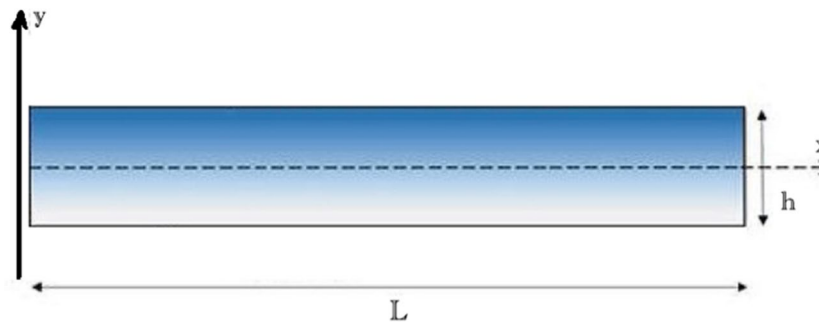


**Figure 1.** Geometry of the considered thermoelectric structure.

computational difficulty of solving complex fractional nonlinear thermoelasticity problems. Numerical methods, including the BEM, should be used to solve such problems. Different three-temperature theories have been investigated in the context of micropolar-thermoelasticity<sup>40</sup>, carbon nanotube fiber reinforced composites<sup>41</sup>, micropolar piezothermoelasticity<sup>42</sup>, Micropolar Magneto-thermoviscoelasticity<sup>43</sup> and Magneto-thermoviscoelasticity<sup>44</sup>. Also, Fahmy introduced new boundary element models for bioheat problems<sup>45</sup>, micropolar composites with temperature-dependent problems<sup>46</sup>, Generalized Porothermoelastic Problems<sup>47</sup> and Size-Dependent thermopiezoelectric Problems<sup>48</sup>.

In this paper, we presented a new fractional order theory of functionally graded magnetic thermoelectric materials. This theory's application to three-temperature nonlinear generalized thermoelasticity is solved using boundary element analysis. Because of its advantages, such as dealing with more complex shapes of functionally graded magnetic thermoelectric materials and not requiring the discretization of the internal domain, BEM has low RAM and CPU usage. As a result, it is adaptable and effective for dealing with complex nonlinear 3 T thermoelectric FGM problems. The numerical results demonstrate the effects of a magnetic field and a graded parameter on thermal stresses in FGM. The numerical results also confirm the validity and accuracy of the proposed technique.

### Formulation of the problem

A Cartesian coordinate system for a 2D functionally graded magnetic thermoelectric structure with thickness of  $h$  and length  $L$  as shown in Fig. 1. It is assumed to be subjected to an electric potential  $\Phi(x, z, t)$  along the  $0x$  direction and placed in an external constant magnetic field  $H_0$  within the region  $R = \{0 < x < L, 0 < y < h\}$  which bounded by boundary  $S$ , where  $S_i$  ( $i = 1, 2, 3, 4$ ) are subsets of  $S$  such that  $S_1 + S_2 = S_3 + S_4 = S$ .

The governing equations for fractional order three-temperature nonlinear generalized thermoelastic problems of functionally graded magnetic thermoelectric materials can be written as<sup>49</sup>

$$\sigma_{ij,j} + \mu_0(x+1)^m \varepsilon_{ijk} J_k H_j = \rho(x+1)^m \ddot{u}_i \quad (1)$$

where

$$\sigma_{ij,j} + \mu_0(x+1)^m \varepsilon_{ijk} J_k H_j = \rho(x+1)^m \ddot{u}_i \quad (2)$$

$$J_i = \sigma_0 (E_i + \varepsilon_{ijk} \dot{u}_k B_j - k_0 T_{,i}) \quad (3)$$

$$B_i = \mu_0 H_i \quad (4)$$

The fractional order three-temperature radiative heat conduction equations coupled with electron, ion and phonon temperatures can be expressed as

$$D_t^\alpha T_\alpha(r, \tau) = \xi \nabla [\mathbb{K}_\alpha \nabla T_\alpha(r, \tau)] + \xi \overline{\overline{W}}(r, \tau), \xi = \frac{1}{c_\alpha \rho \delta_1} \quad (5)$$

where

$$\overline{\overline{W}}(r, \tau) = \begin{cases} -\rho \mathbb{W}_{ei}(T_e - T_i) - \rho \mathbb{W}_{ep}(T_e - T_p) + \overline{\overline{W}}(r, \tau), & \alpha = e, \delta_1 = 1 \\ \rho \mathbb{W}_{ei}(T_e - T_i) + \overline{\overline{W}}(r, \tau), & \alpha = i, \delta_1 = 1 \\ \rho \mathbb{W}_{ep}(T_e - T_p) + \overline{\overline{W}}(r, \tau), & \alpha = p, \delta_1 = \frac{4}{\rho} T_p^3 \end{cases} \quad (6)$$

in which

$$\overline{\overline{W}}(r, \tau) = -\delta_{2j} \mathbb{K}_\alpha \dot{T}_{\alpha,ab} + \beta_{ab} T_{\alpha 0} [\delta_{1j} \dot{u}_{a,b} + (\tau_0 + \delta_{2j}) \ddot{u}_{a,b}] + \rho c_\alpha [(\tau_0 + \delta_{1j} \tau_2 + \delta_{2j}) \ddot{T}_\alpha] - \rho \pi_0 J_{i,j}$$

and

$$\mathbb{W}_{ei} = \rho \mathbb{A}_{ei} T_e^{-2/3}, \mathbb{W}_{ep} = \rho \mathbb{A}_{ep} T_e^{-1/2}, \mathbb{K}_\alpha = \mathbb{A}_\alpha T_\alpha^{5/2}, \alpha = e, i, \mathbb{K}_p = \mathbb{A}_p T_p^{3+\mathbb{B}} \tag{7}$$

The total energy of a unit mass can be described as follows:

$$P = P_e + P_i + P_p, P_e = c_e T_e, P_i = c_i T_i, P_p = \frac{1}{\rho} c_p T_p^4 \tag{8}$$

Initial and boundary conditions can be written as

$$T_\alpha(x, y, 0) = T_\alpha^0(x, y) = g_1(x, \tau) \tag{9a}$$

$$\mathbb{K}_\alpha \frac{\partial T_\alpha}{\partial n} \Big|_{\Gamma_1} = 0, \alpha = e, i, T_p \Big|_{\Gamma_1} = g_2(x, \tau) \tag{9b}$$

$$\mathbb{K}_\alpha \frac{\partial T_\alpha}{\partial n} \Big|_{\Gamma_2} = 0, \alpha = e, i, p \tag{9c}$$

### BEM simulation for temperature field

The boundary element method is used in this section to solve the nonlinear time-dependent two dimensions three temperature (2D-3 T) radiation diffusion equations that are coupled by electron, ion, and photon temperatures.

Caputo’s integral definition and Grunwald–Letnikov integral definition are consistent with the Riemann–Liouville integral definition. Also, Caputo’s derivative definition and Grunwald–Letnikov derivative definition are consistent with the Riemann–Liouville derivative definition. When the Riemann–Liouville or Grunwald–Letnikov definitions are compared to the Caputo definition, the functions that are derivable in the Caputo sense are significantly fewer. According to finite difference scheme of Caputo at times  $(f + 1)\Delta\tau$  and  $f\Delta\tau$ , we obtain<sup>50</sup>

$$D_\tau^a T_\alpha^{f+1} + D_\tau^a T_\alpha^f \approx \sum_{j=0}^k W_{a,j} \left( T_\alpha^{f+1-j}(r) - T_\alpha^{f-j}(r) \right), (f = 1, 2, \dots, F) \tag{10}$$

where

$$W_{a,0} = \frac{(\Delta\tau)^{-a}}{\Gamma(2-a)}, W_{a,j} = W_{a,0} \left( (j+1)^{1-a} - (j-1)^{1-a} \right), j = 1, 2, \dots, F \tag{11}$$

Based on Eq. (10), the fractional order heat Eqs. (5) can be replaced by the following system

$$\begin{aligned} & W_{a,0} T_\alpha^{f+1}(r) - \mathbb{K}_\alpha(x) T_{\alpha,II}^{f+1}(r) - \mathbb{K}_{\alpha,I}(x) T_{\alpha,I}^{f+1}(r) \\ & = W_{a,0} T_\alpha^f(r) - \mathbb{K}_\alpha(x) T_{\alpha,II}^f(r) \\ & - \mathbb{K}_{\alpha,I}(x) T_{\alpha,I}^f(r) - \sum_{j=1}^f W_{a,j} \left( T_\alpha^{f+1-j}(r) - T_\alpha^{f-j}(r) \right) \\ & + \bar{\mathbb{W}}_m^{f+1}(x, \tau) + \bar{\mathbb{W}}_m^f(x, \tau), f = 0, 1, 2, \dots, F \end{aligned} \tag{12}$$

Based on the fundamental solution of (12), the direct formulation of boundary integral equation corresponding to (5) can be expressed as

$$CT_\alpha = \frac{D}{\mathbb{K}_\alpha} \int_S \int_0^\tau [T_\alpha q^* - T_\alpha^* q] dS d\tau + \frac{D}{\mathbb{K}_\alpha} \int_R \int_0^\tau b T_\alpha^* dR d\tau + \int_R T_\alpha^i T_\alpha^* \Big|_{\tau=0} dR \tag{13}$$

which can be written in the absence of internal heat sources as follows

$$CT_\alpha = \int_S [T_\alpha q^* - T_\alpha^* q] dS - \int_R \frac{\mathbb{K}_\alpha}{D} \frac{\partial T_\alpha^*}{\partial \tau} T_\alpha dR \tag{14}$$

We assume that the time derivative of temperature can be approximated by a series of known functions in order to transform the domain integral in (14) to the boundary.  $f^j(r)$  and unknown coefficients  $a^j(\tau)$  as

$$\frac{\partial T_\alpha}{\partial \tau} \cong \sum_{j=1}^N f^j(r) a^j(\tau) \tag{15}$$

Also, we assume that  $\hat{T}_\alpha^j$  is a solution of

$$\nabla^2 \hat{T}_\alpha^j = f^j \tag{16}$$

Thus, Eq. (14) results in the following boundary integral equation

$$CT = \int_S [T_\alpha q^* - T_\alpha^* q] dS + \sum_{j=1}^N a^j(\tau) D^{-1} \left( C \hat{T}_\alpha^j - \int_S [T_\alpha^j q^* - \hat{q}^j T_\alpha^*] dS \right) \tag{17}$$

where

$$\hat{q}^j = -\mathbb{K}_\alpha \frac{\partial \hat{T}_\alpha^j}{\partial n} \tag{18}$$

and

$$a^j(\tau) = \sum_{i=1}^N f_{ji}^{-1} \frac{\partial T(r_i, \tau)}{\partial \tau} \tag{19}$$

In which the entries of  $f_{ji}^{-1}$  are the coefficients of  $F^{-1}$  with matrix  $F$  defined as<sup>51</sup>

$$\{F\}_{ji} = f^j(r_i) \tag{20}$$

Using the standard boundary element discretization scheme for Eq. (17) and using Eq. (19), we obtain the following set of ordinary differential equations

$$C\dot{T}_\alpha + HT_\alpha = GQ \tag{21}$$

where matrices  $H$  and  $G$  are depending on the current time step, boundary geometry and material properties,  $T_\alpha$  and  $Q$  are, respectively, temperature and heat flux vectors at boundary nodes, and  $b$  is the internal heat generation vector.

The diffusion matrix can be defined as

$$C = -[H\hat{T}_\alpha - G\hat{Q}]F^{-1}D^{-1} \tag{22}$$

with

$$\{\hat{T}\}_{ij} = \hat{T}^j(x_i) \tag{23}$$

$$\{\hat{Q}\}_{ij} = \hat{q}^j(x_i) \tag{24}$$

In order to solve Eq. (21) numerically the functions  $T_\alpha$  and  $q$  are interpolated as

$$T_\alpha = (1 - \theta)T_\alpha^m + \theta T_\alpha^{m+1} \tag{25}$$

$$q = (1 - \theta)q^m + \theta q^{m+1} \tag{26}$$

where the parameter  $\theta = \frac{\tau - \tau^m}{\tau^{m+1} - \tau^m}$ ,  $0 \leq \theta \leq 1$  determines the practical time  $\tau$  in the present time step.

By differentiating Eq. (25) with respect to time we get

$$\dot{T}_\alpha = \frac{dT_\alpha}{d\theta} \frac{d\theta}{d\tau} = \frac{T_\alpha^{m+1} - T_\alpha^m}{\tau^{m+1} - \tau^m} = \frac{T_\alpha^{m+1} - T_\alpha^m}{\Delta\tau^m} \tag{27}$$

By substituting from Eqs. (25)–(27) into Eq. (21), we obtain

$$\left( \frac{C}{\Delta\tau^m} + \theta H \right) T_\alpha^{m+1} - \theta GQ^{m+1} = \left( \frac{C}{\Delta\tau^m} - (1 - \theta)H \right) T_\alpha^m + (1 - \theta)GQ^m \tag{28}$$

By using initial and boundary conditions at  $\Delta\tau^m$  and considering the previous time step solution as initial values for the next step, we obtain the following linear algebraic system

$$aX = b \tag{29}$$

where  $a$  is unknown matrix, and  $X$  and  $b$  are known matrices.

### BEM simulation for displacement and microrotation fields

Using the weighted residual method, the governing Eqs. (1) and (2) can be transformed into the following integral equations

$$\int_R (\sigma_{ij,j} + U_i) u_i^* dR = 0 \tag{30}$$

in which

$$U_i = \mu_0(x + 1)^m \varepsilon_{ijk} J_k H_j - \rho \ddot{u}_i \tag{31}$$

The boundary conditions are

$$u_i = \bar{u}_i \quad \text{on } S_1 \tag{32}$$

$$\lambda_i = \sigma_{ij} n_j = \bar{\lambda}_i \quad \text{on } S_2 \tag{33}$$

The integration of the first term of Eqs. (33) and (34) leads to

$$-\int_R \sigma_{ij} u_{ij}^* dR + \int_R U_i u_i^* dR = -\int_{S_2} \lambda_i u_i^* dS \tag{34}$$

According to Huang and Liang<sup>52</sup>, the boundary integral equation can be written as

$$-\int_R \sigma_{ij} u_{ij}^* dR + \int_R U_i u_i^* dR = \int_{S_2} (\lambda_i - \bar{\lambda}_i) u_i^* dS + \int_{S_1} (\bar{u}_i - u_i) \lambda_i^* dS \tag{35}$$

The integration of (35)'s left-hand side by parts results in

$$-\int_R \sigma_{ij}^* \varepsilon_{ij}^* dR + \int_R U_i u_i^* dR = -\int_{S_2} \bar{\lambda}_i u_i^* dS - \int_{S_1} \lambda_i u_i^* dS + \int_{S_1} (\bar{u}_i - u_i) \lambda_i^* dS \tag{36}$$

According to Eringen<sup>53</sup>, the elastic stress can be written as

$$\sigma_{ij} = \mathbb{A}_{ijkl} \varepsilon_{kl}, \quad \text{where } \mathbb{A}_{ijkl} = \mathbb{A}_{klij} \tag{37}$$

Hence, Eq. (36) may be expressed as

$$-\int_R \sigma_{ij}^* \varepsilon_{ij}^* dR + \int_R U_i u_i^* dR = -\int_{S_2} \bar{\lambda}_i u_i^* dS - \int_{S_1} \lambda_i u_i^* dS + \int_{S_1} (\bar{u}_i - u_i) \lambda_i^* dS \tag{38}$$

By applying the integration by parts again to the left-hand side of (38), we obtain

$$\int_R \sigma_{ij,j}^* u_i dR = -\int_S u_i^* \lambda_i dS + \int_S \lambda_i^* u_i dS \tag{39}$$

where

$$\sigma_{ij,j}^* + \Delta^n e_l = 0 \tag{40}$$

According to Dragos<sup>54</sup>, the fundamental solution may be written as

$$u_i^* = u_{li}^* e_l, \quad \lambda_i^* = \lambda_{li}^* e_l, \tag{41}$$

The weighting functions for  $U_i = 0$  and  $V_i = \Delta^n$  may be expressed as follows:

$$\sigma_{ij,j}^{**} = 0 \tag{42}$$

On the basis of Dragos<sup>54</sup>, the fundamental solution may be expressed as

$$u_i^* = u_{li}^{**} e_l, \quad \lambda_i^* = \lambda_{li}^{**} e_l \tag{43}$$

Using the above two sets of weighting functions into (39) we have

$$C_{li}^n u_i^n = -\int_S \lambda_{li}^* u_i dS + \int_S u_{li}^* \lambda_i dS \tag{44}$$

$$C_{li}^n \omega_i^n = -\int_S \lambda_{li}^{**} u_i dS + \int_S u_{li}^{**} \lambda_i dS \tag{45}$$

Thus, we obtain

$$C^n = -\int_S \mathbb{P}^* \mathbb{Q} dS + \int_S \mathbb{Q}^* \mathbb{P} dS \tag{46}$$

in which

$$C^n = \begin{bmatrix} C_{11} & C_{12} \\ C_{21} & C_{22} \end{bmatrix}, \quad \mathbb{Q}^* = \begin{bmatrix} u_{11}^* & u_{12}^* \\ u_{21}^* & u_{22}^* \end{bmatrix}, \quad \mathbb{P}^* = \begin{bmatrix} \lambda_{11}^* & \lambda_{12}^* \\ \lambda_{21}^* & \lambda_{22}^* \end{bmatrix}, \quad \mathbb{Q} = \begin{bmatrix} u_1 \\ u_2 \end{bmatrix}, \quad \mathbb{P} = \begin{bmatrix} \lambda_1 \\ \lambda_2 \end{bmatrix} \subseteq \tag{47}$$

Now, we introduce the following relations

$$\mathbb{P} = \psi q^j, \quad \mathbb{P} = \psi p^j \tag{48}$$

By discretizing the boundary, we can write (46) as

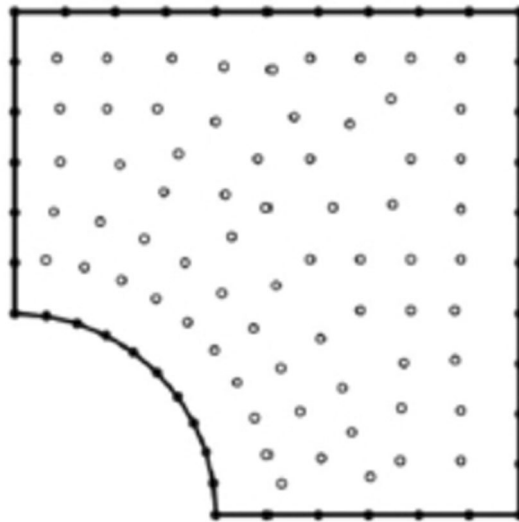


**Figure 2.** Boundary element model of the considered structure.

$$C^n \mathbf{q}^n = \sum_{j=1}^{N_e} \left[ - \int_{\Gamma_j} \mathbb{P}^* \psi d\Gamma \right] \mathbf{q}^j + \sum_{j=1}^{N_e} \left[ \int_{\Gamma_j} \mathbf{q}^* \psi d\Gamma \right] \mathbb{P}^j \tag{49}$$

which can be expressed as

$$C^i \mathbf{q}^i = - \sum_{j=1}^{N_e} \hat{\mathbb{H}}^{ij} \mathbf{q}^j + \sum_{j=1}^{N_e} \hat{\mathbb{G}}^{ij} \mathbb{P}^j \tag{50}$$

By employing the following formula

$$\mathbb{H}^{ij} = \begin{cases} \hat{\mathbb{H}}^{ij} & \text{if } i \neq j \\ \hat{\mathbb{H}}^{ij} + C^i & \text{if } i = j \end{cases} \tag{51}$$

Hence, Eq. (50) may be expressed as

$$\sum_{j=1}^{N_e} \mathbb{H}^{ij} \mathbf{q}^j = \sum_{j=1}^{N_e} \hat{\mathbb{G}}^{ij} \mathbb{P}^j \tag{52}$$

The global matrix system equation for all  $i$  nodes can be written as follows

$$\mathbb{H}\mathbf{Q} = \mathbb{G}\mathbb{P} \tag{53}$$

where  $\mathbf{Q}$  denotes the displacements and  $\mathbb{P}$  denotes the tractions.

Now, we can write (53) into the following form

$$\mathbb{A}\mathbf{X} = \mathbb{B} \tag{54}$$

In Matlab (R2018a), an explicit staggered predictor–corrector scheme based on the communication-avoiding generalized minimal residual (CA-GMRES) method is efficiently implemented for solving the resulting simultaneous linear algebraic systems to obtain the temperature and displacement fields<sup>37</sup>.

### Numerical results and discussion

In the context of functionally graded magnetic thermoelectric materials, the proposed BEM technique can be applied to a wide range of fractional-order nonlinear generalised thermal stress problems. The BEM discretization was performed using 42 boundary elements and 68 internal points, as shown in Fig. 2.

Figure 3 shows the variation of the thermal stress  $\sigma_{11}$  along  $x$ -axis for different values of fractional order parameter ( $a = 0.3, 0.6$  and  $0.9$ ). It is shown from this figure that the thermal stress  $\sigma_{11}$  decreases with the increase of  $x$  until  $x = 0.9$ . Then it increases with the increase of  $x$ . It is also shown from this figure that the thermal stress  $\sigma_{11}$  decreases with the increase of fractional order parameter.

Figure 4 shows the variation of the thermal stress  $\sigma_{12}$  along  $x$ -axis for different values of fractional order parameter ( $a = 0.3, 0.6$  and  $0.9$ ). It is shown from this figure that the thermal stress  $\sigma_{12}$  decreases with the increase of  $x$ . It is also shown from this figure that the thermal stress  $\sigma_{21}$  increases with the increase of fractional order parameter.

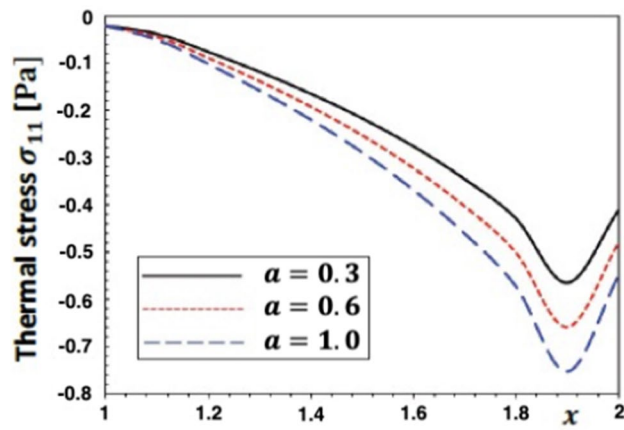


Figure 3. Variation of the thermal stress  $\sigma_{11}$  along  $x$ -axis for different values of fractional order parameter.

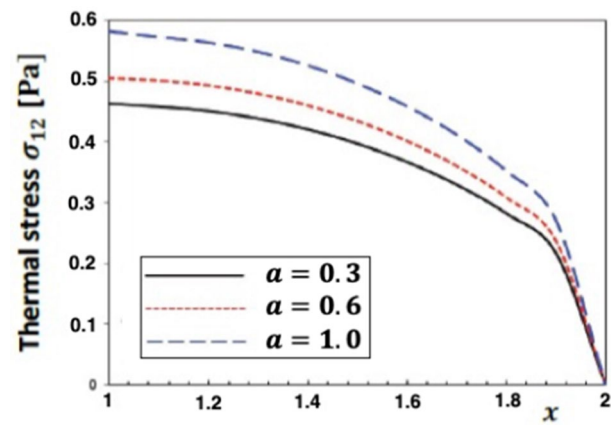


Figure 4. Variation of the thermal stress  $\sigma_{12}$  along  $x$ -axis for different values of fractional order parameter.

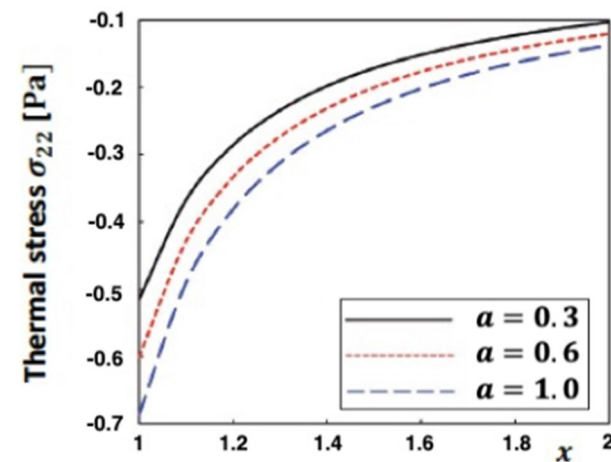
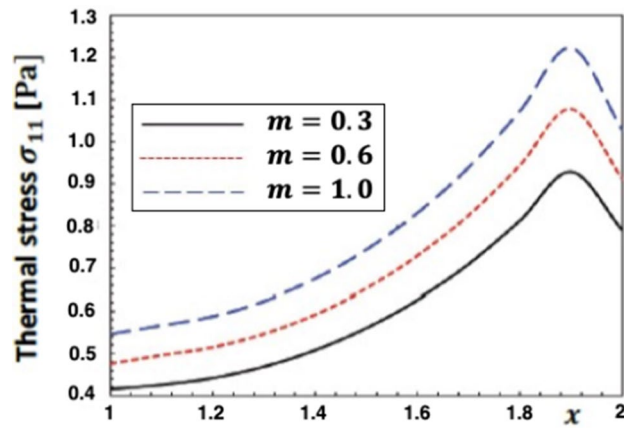
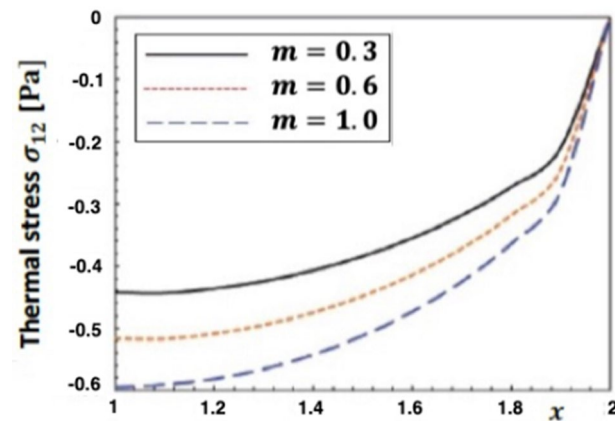


Figure 5. Variation of the thermal stress  $\sigma_{22}$  along  $x$ -axis for different values of fractional order parameter.



**Figure 6.** Variation of the thermal stress  $\sigma_{11}$  along  $x$ -axis for different values of functionally graded parameter.



**Figure 7.** Variation of the thermal stress  $\sigma_{12}$  along  $x$ -axis for different values of functionally graded parameter.

Figure 5 shows the variation of the thermal stress  $\sigma_{22}$  along  $x$ -axis for different values of fractional order parameter ( $a = 0.3, 0.6$  and  $0.9$ ). It is shown from this figure that the thermal stress  $\sigma_{22}$  increases with the increase of  $x$ . It is also shown from this figure that the thermal stress  $\sigma_{22}$  decreases with the increase of fractional order parameter.

Figure 6 shows the variation of the thermal stress  $\sigma_{11}$  along  $x$ -axis for different values of functionally graded parameter ( $m = 0.3, 0.6$  and  $0.9$ ). It is shown from this figure that the thermal stress  $\sigma_{11}$  increases with the increase of  $x$  until  $x = 0.9$ . Then it decreases with the increase of  $x$ . It is also shown from this figure that the thermal stress  $\sigma_{11}$  increases with the increase of functionally graded parameter.

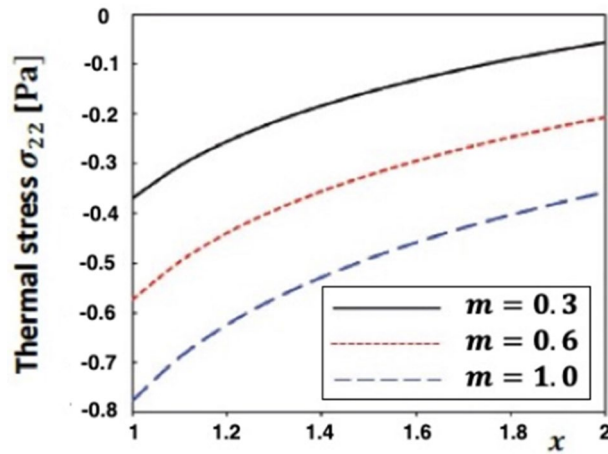
Figure 7 shows the variation of the thermal stress  $\sigma_{12}$  along  $x$ -axis for different values of functionally graded parameter ( $m = 0.3, 0.6$  and  $0.9$ ). It is shown from this figure that the thermal stress  $\sigma_{12}$  increases with the increase of  $x$ . It is also shown from this figure that the thermal stress  $\sigma_{21}$  decreases with the increase of functionally graded parameter.

Figure 8 shows the variation of the thermal stress  $\sigma_{22}$  along  $x$ -axis for different values of functionally graded parameter ( $m = 0.3, 0.6$  and  $0.9$ ). It is shown from this figure that the thermal stress  $\sigma_{22}$  increases with the increase of  $x$ . It is also shown from this figure that the thermal stress  $\sigma_{22}$  decreases with the increase of functionally graded parameter.

It is noted from Figs. 3, 4, 5, 6, 7 and 8 that the fractional order parameter and functionally graded parameter have a strong effect on the thermal stress  $\sigma_{11}$ ,  $\sigma_{12}$  and  $\sigma_{22}$  in the functionally graded magnetic thermoelectric materials.

Table 1 shows a comparison of required computer resources for the current BEM results, GFDM results of Gu et al.<sup>55</sup> and FEM–NMM results of An et al.<sup>56</sup> of modeling of fractional nonlinear three-temperature (3 T) thermoelectric problems.

There were no published results to demonstrate the validity of the proposed technique's results. Some literatures, on the other hand, can be regarded as special cases of the considered general study. Figure 9 shows the variation of the special case thermal stress  $\sigma_{11}$  along  $x$ -axis for BEM, generalized finite difference method (GFDM) and combined finite element method/normal mode method (FEM–NMM) in the case of fractional



**Figure 8.** Variation of the thermal stress  $\sigma_{22}$  along  $x$ -axis for different values of functionally graded parameter.

	BEM	GFDM	FEM–NMM
Number of nodes	68	50,000	48,000
Number of elements	42	20,000	18,000
CPU time	2	200	180
Memory	1	180	160
Disc space	0	240	220
Accuracy of results	1	2.2	2.0

**Table 1.** A comparison of the required computer resources for modeling of fractional nonlinear three-temperature (3 T) thermoelectric problems.

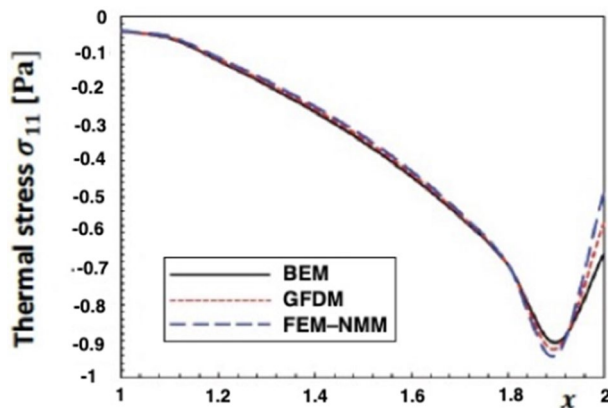


**Figure 9.** Variation of the special case thermal stress  $\sigma_{11}$  along  $x$ -axis for BEM, GFDM and FEM–NMM ( $a = 0.6, m = 0.0$ ).

order ( $a = 0.6$ ) homogeneous ( $m = 0.0$ ). Figure 10 shows the propagation of the thermal stress  $\sigma_{11}$  along  $x$ -axis for BEM, GFDM and FEM–NMM in the case of zero fractional order, ( $a = 0.0$ ) and non-homogeneous ( $m = 0.6$ ). These findings for thermal stress  $\sigma_{11}$  in functionally graded magnetic thermoelectric materials, show that the BEM findings are in a very good agreement with the GFDM findings of Gu et al.<sup>55</sup>, and FEM–NMM findings of An et al.<sup>56</sup>. These results show that the BEM results are in a very good agreement to the FEM and NMM results. Thus, the validity of the proposed technique was confirmed.

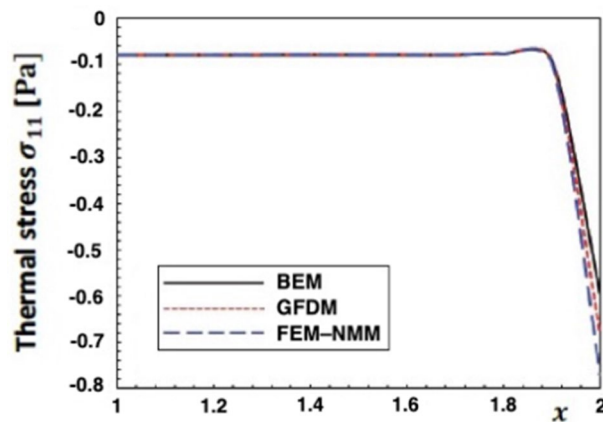


**Figure 10.** Variation of the special case thermal stress  $\sigma_{11}$  along  $x$ -axis for BEM, GFDM and FEM–NMM ( $a = 0.0, m = 0.6$ ).

## Conclusion

Based on an explicit staggered predictor–corrector scheme The primary goal of this paper is to present a novel fractional-order theory that will aid in the advancement of functionally graded magnetic thermoelectric materials’ technological and industrial applications. Three-temperature nonlinear generalized thermoelasticity of functionally graded magnetic thermoelectric materials is the name given to this theory (FGMTMs). We must successfully adopt computerized numerical methods for solving and simulating complex nonlinear FGM problems in order to successfully guide the current research field toward the development of new functionally graded materials (FGMs). The governing equations are extremely difficult to solve experimentally or analytically due to the proposed theory’s severe nonlinearity. To address this issue, new numerical approaches for solving such equations must be developed. We propose a new formulation of the boundary element method for solving the theory’s governing equations (BEM). Because of the advantages of the BEM approach, such as the ability to deal with issues with complicated shapes that are difficult to deal with using standard methods, and the lack of the need for internal domain discretization. It also necessitates low CPU utilization and memory storage. As a result, the BEM is appropriate for a wide variety of sophisticated FGMTMs applications. The numerical results are discussed, with an emphasis on the effects of magnetic fields and graded parameters on thermal stresses in FGMTMs. Based on the findings, the suggested BEM technique is more effective, precise, and stable than GFDM or FEM–NMM. Current numerical results for our problem may be of interest to computer scientists, material science researchers, engineers, and designers and developers of functionally graded materials.

## Data availability

All data generated or analysed during this study are included in this published article.

Received: 11 February 2022; Accepted: 5 April 2022

Published online: 26 April 2022

## References

- Cheng, S., Wei, Y., Sheng, D., Chen, Y. & Wang, Y. Identification for hammerstein nonlinear ARMAX systems based on multi-innovation fractional order stochastic gradient. *Signal Process.* **142**, 1–10 (2018).
- Chaudhary, N. I., Zubair, S., Raja, M. A. Z. & Dedovic, N. Normalized fractional adaptive methods for nonlinear control autoregressive systems. *Appl. Math. Model.* **66**, 457–471 (2019).
- Khan, Z. A., Zubair, S., Alquhayz, H., Azeem, M. & Ditta, A. Design of momentum fractional stochastic gradient descent for recommender systems. *IEEE Access* **7**, 179575–179590 (2019).
- Sabatier, J., Agrawal, O. P. & Machado, J. T. *Advances in Fractional Calculus* (Springer, 2007).
- Bertsias, P., Psychalinos, C., Maundy, B. J., Elwakil, A. S. & Radwan, A. G. Partial fraction expansion based realizations of fractional order differentiators and integrators using active filters. *Int. J. Circ. Theory Appl.* **47**, 513–531 (2019).
- Machado, J. T. & Lopes, A. M. Artistic painting: A fractional calculus perspective. *Appl. Math. Model.* **65**, 614–626 (2019).
- Tang, Y., Zhen, Y. & Fang, B. Nonlinear vibration analysis of a fractional dynamic model for the viscoelastic pipe conveying fluid. *Appl. Math. Model.* **56**, 123–136 (2018).
- Long, Y., Xu, B., Chen, D. & Ye, W. Dynamic characteristics for a hydro-turbine governing system with viscoelastic materials described by fractional calculus. *Appl. Math. Model.* **58**, 128–139 (2018).
- Baleanu, D. & Machado, J. A. T. *Fractional Dynamics and Control* (Springer Science & Business Media, 2011).
- Sharma, R., Bhasin, S., Gaur, P. & Joshi, D. A switching-based collaborative fractional order fuzzy logic controllers for robotic manipulators. *Appl. Math. Model.* **73**, 228–246 (2019).
- Baleanu, D. et al. (eds) *New Trends in Nanotechnology and Fractional Calculus Applications* C397 (Springer, 2010).
- Pinto, C. M. & Carvalho, A. R. Diabetes mellitus and TB co-existence: Clinical implications from a fractional order modelling. *Appl. Math. Model.* **68**, 219–243 (2019).
- Ionescu, C., Lopes, A., Copot, D., Machado, J. T. & Bates, J. H. T. The role of fractional calculus in modeling biological phenomena: A review. *Commun. Nonlinear Sci. Numer. Simul.* **51**, 141–159 (2017).
- Chaudhary, N. I., Zubair, S. & Raja, M. A. Z. A new computing approach for power signal modeling using fractional adaptive algorithms. *ISA Trans.* **68**, 189–202 (2017).

15. Zubair, S., Chaudhary, N. I., Khan, Z. A. & Wang, W. Momentum fractional LMS for power signal parameter estimation. *Signal Process.* **142**, 441–449 (2018).
16. Cheng, S., Wei, Y., Chen, Y., Li, Y. & Wang, Y. An innovative fractional order LMS based on variable initial value and gradient order. *Signal Process.* **133**, 260–269 (2017).
17. Hussanan, A., Salleh, M. Z., Khan, I. & Shafie, S. Convection heat transfer in micropolar nanofluids with oxide nanoparticles in water, kerosene and engine oil. *J. Mol. Liq.* **229**, 482–488 (2017).
18. Aman, S., Khan, I., Ismail, Z., Salleh, M. Z. & Al-Mdallal, Q. M. Heat transfer enhancement in free convection flow of CNTs Maxwell nanofluids with four different types of molecular liquids. *Sci. Rep.* **7**, 2445 (2017).
19. Sheikholeslami, M., Shah, Z., Shafee, A., Khan, I. & Tlili, I. Uniform magnetic force impact on water based nanofluid thermal behavior in a porous enclosure with ellipse shaped obstacle. *Sci. Rep.* **9**, 1196 (2019).
20. Khan, N. S. *et al.* Magneto-hydrodynamic nanoliquid thin film sprayed on a stretching cylinder with heat transfer. *Appl. Sci.* **7**, 271 (2017).
21. Aaiza, G., Khan, I. & Shafie, S. Energy transfer in mixed convection MHD flow of nanofluid containing different shapes of nanoparticles in a channel filled with saturated porous medium. *Nanoscale Res. Lett.* **10**, 490 (2015).
22. Nazeer, M. *et al.* Theoretical study of MHD electro-osmotically flow of third-grade fluid in micro channel. *Appl. Math. Comput.* **420**, 126868. <https://doi.org/10.1016/j.amc.2021.126868> (2022).
23. Chu, Y. M. *et al.* Combined impact of Cattaneo-Christov double diffusion and radiative heat flux on bio-convective flow of Maxwell liquid configured by a stretched nano-material surface. *Appl. Math. Comput.* **419**, 126883. <https://doi.org/10.1016/j.amc.2021.126883> (2022).
24. Zhao, T. H., Khan, M. I. & Chu, Y. M. Artificial neural networking (ANN) analysis for heat and entropy generation in flow of non-Newtonian fluid between two rotating disks. *Math. Methods Appl. Sci.* <https://doi.org/10.1002/mma.7310> (2021).
25. Wang, J., Khan, M. I., Khan, W. A., Abbas, S. Z. & Khan, M. I. Transportation of heat generation/absorption and radiative heat flux in homogeneous–heterogeneous catalytic reactions of non-Newtonian fluid (Oldroyd-B model). *Comput. Methods Progr. Biomed.* **189**, 105310 (2020).
26. Khan, M. I., Qayyum, S., Kadry, S., Khan, W. A. & Abbas, S. Z. Irreversibility analysis and heat transport in squeezing nanoliquid flow of non-Newtonian (second-grade) fluid between infinite plates with activation energy. *Arab. J. Sci. Eng.* **45**, 4939–4947 (2020).
27. Raja, M. A. Z. *et al.* Intelligent computing through neural networks for entropy generation in MHD third-grade nanofluid under chemical reaction and viscous dissipation. *Waves Random Complex Media* <https://doi.org/10.1080/17455030.2022.2044095> (2022).
28. Knopoff, L. The interaction between elastic wave motions and a magnetic field in electrical conductors. *J. Geophys. Res.* **60**, 441–456 (1955).
29. Chadwick, P. *Thermoelasticity. The Dynamical Theory, Progress in Solid Mechanics* Vol. 1, 263–328 (North-Holland Publishing Co, 1960).
30. Kaliski, S. & Petykiewicz, J. Equation of motion coupled with the field of temperature in a magnetic field involving mechanical and electrical relaxation for anisotropic bodies. *Proc. Vib. Probl.* **1**, 3–11 (1959).
31. Fahmy, M. A. A time-stepping DRBEM for magneto-thermo-viscoelastic interactions in a rotating nonhomogeneous anisotropic solid. *Int. J. Appl. Mech.* **3**, 1–24 (2011).
32. Fahmy, M. A. A time-stepping DRBEM for the transient magneto-thermo-visco-elastic stresses in a rotating non-homogeneous anisotropic solid. *Eng. Anal. Bound. Elem.* **36**, 335–345 (2012).
33. Fahmy, M. A. The effect of rotation and inhomogeneity on the transient magneto-thermoviscoelastic stresses in an anisotropic solid. *ASME J. Appl. Mech.* **79**, 1015 (2012).
34. Fahmy, M. A. Implicit-Explicit time integration DRBEM for generalized magneto-thermoelasticity problems of rotating anisotropic viscoelastic functionally graded solids. *Eng. Anal. Bound. Elem.* **37**, 107–115 (2013).
35. Fahmy, M. A. Generalized magneto-thermo-viscoelastic problems of rotating functionally graded anisotropic plates by the dual reciprocity boundary element method. *J. Therm. Stress.* **36**, 1–20 (2013).
36. Fahmy, M. A. Transient magneto-thermoviscoelastic plane waves in a non-homogeneous anisotropic thick strip subjected to a moving heat source. *Appl. Math. Model.* **36**, 4565–4578 (2012).
37. Fahmy, M. A. A new boundary element strategy for modeling and simulation of three temperatures nonlinear generalized micropolar-magneto-thermoelastic wave propagation problems in FGA structures. *Eng. Anal. Bound. Elem.* **108**, 192–200 (2019).
38. Fahmy, M. A. A Computerized DRBEM model for generalized magneto-thermo-visco-elastic stress waves in functionally graded anisotropic thin film/substrate structures. *Latin Am. J. Solids Struct.* **11**, 386–409 (2014).
39. Ezzat, M. A. & Awad, E. S. Micropolar generalized magneto-thermoelasticity with modified Ohm's and Fourier's laws. *J. Math. Anal. Appl.* **353**, 99–113 (2009).
40. Fahmy, M. A. A novel BEM for modeling and simulation of 3T nonlinear generalized anisotropic micropolar-thermoelasticity theory with memory dependent derivative. *CMES-Comput. Model. Eng. Sci.* **126**, 175–199 (2021).
41. Fahmy, M. A. A new boundary element formulation for modeling and simulation of three-temperature distributions in carbon nanotube fiber reinforced composites with inclusions. *Math. Methods Appl. Sci.* <https://doi.org/10.1002/mma.7312> (2021).
42. Fahmy, M. A. Boundary element algorithm for nonlinear modeling and simulation of three temperature anisotropic generalized micropolar piezothermoelasticity with memory-dependent derivative. *Int. J. Appl. Mech.* **12**, 2050027 (2020).
43. Fahmy, M. A. *et al.* Boundary element modeling for simulation and optimization of three-temperature anisotropic micropolar magneto-thermoviscoelastic problems in porous smart structures using NURBS and genetic algorithm. *Int. J. Thermophys.* **42**, 29 (2019).
44. Fahmy, M. A. Boundary element modeling of 3T nonlinear transient magneto-thermoviscoelastic wave propagation problems in anisotropic circular cylindrical shells. *Compos. Struct.* **27**, 114655. <https://doi.org/10.1016/j.compstruct.2021.114655> (2021).
45. Fahmy, M. A. A new boundary element algorithm for a general solution of nonlinear space-time fractional dual-phase-lag bio-heat transfer problems during electromagnetic radiation. *Case Stud. Therm. Eng.* **25**, 100918. <https://doi.org/10.1016/j.csite.2021.100918> (2021).
46. Fahmy, M. A. A new boundary element algorithm for modeling and simulation of nonlinear thermal stresses in micropolar FGA composites with temperature-dependent properties. *Adv. Model. Simul. Eng. Sci.* **8**, 1–23. <https://doi.org/10.1186/s40323-021-00193-6> (2021).
47. Fahmy, M. A. A new BEM for fractional nonlinear generalized prothermoelastic wave propagation problems. *CMC Comput. Mater. Contin.* **68**(1), 59–76. <https://doi.org/10.32604/cmc.2021.015115> (2021).
48. Fahmy, M. A. A new BEM modeling algorithm for size-dependent thermopiezoelectric problems in smart nanostructures. *CMC Comput. Mater. Contin.* **69**, 931–944. <https://doi.org/10.32604/cmc.2021.018191> (2021).
49. Fahmy, M. A. Implicit–explicit time integration DRBEM for generalized magneto-thermo-elasticity problems of rotating anisotropic viscoelastic functionally graded solids. *Eng. Anal. Bound. Elem.* **37**, 107–115 (2013).
50. Cattaneo, C. Sur une forme de l'équation de la chaleur éliminant le paradoxe d'une propagation instantanée. *Comptes Rendus de l'Académie des Sci.* **247**, 431–433 (1958).
51. Fahmy, M. A. Boundary element modeling of fractional nonlinear generalized photothermal stress wave propagation problems in FG anisotropic smart semiconductors. *Eng. Anal. Bound. Elem.* **134**, 665–679. <https://doi.org/10.1016/j.enganabound.2021.11.009> (2022).
52. Huang, F. Y. & Liang, K. Z. Boundary element method for micropolar thermoelasticity. *Eng. Anal. Bound. Elem.* **17**, 19–26 (1996).

53. Eringen, A. C. *Theory of Micropolar Elasticity. Fracture II* (Academic Press, 1968).
54. Dragos, L. Fundamental solutions in micropolar elasticity. *Int. J. Eng. Sci.* **22**, 265–275 (1984).
55. Gu, Y., Qu, W., Chen, W., Song, L. & Zhang, Ch. The generalized finite difference method for long-time dynamic modeling of three-dimensional coupled thermoelasticity problems. *J. Comput. Phys.* **384**, 42–59. <https://doi.org/10.1016/j.jcp.2019.01.027> (2019).
56. An, B., Zhang, C., Shang, D., Xiao, Y. & Khan, I. U. A combined finite element method with normal mode for the elastic structural acoustic radiation in shallow water. *J. Theor. Comput. Acoust.* **28**(04), 2050004 (2020).

## Acknowledgements

The authors would like to thank the Deanship of Scientific Research at Umm Al-Qura University for supporting this work by Grant Code: (22UQU4340548DSR03).

## Author contributions

First Author suggested the problem and solution. All authors wrote the main text and reviewed the manuscript.

## Funding

This research was funded by [Deanship of Scientific Research at Umm Al-Qura University] grant number [22UQU4340548DSR03] And The APC was funded by [Deanship of Scientific Research at Umm Al-Qura University].

## Competing interests

The authors declare no competing interests.

## Additional information

**Correspondence** and requests for materials should be addressed to M.A.F.

**Reprints and permissions information** is available at [www.nature.com/reprints](http://www.nature.com/reprints).

**Publisher's note** Springer Nature remains neutral with regard to jurisdictional claims in published maps and institutional affiliations.



**Open Access** This article is licensed under a Creative Commons Attribution 4.0 International License, which permits use, sharing, adaptation, distribution and reproduction in any medium or format, as long as you give appropriate credit to the original author(s) and the source, provide a link to the Creative Commons licence, and indicate if changes were made. The images or other third party material in this article are included in the article's Creative Commons licence, unless indicated otherwise in a credit line to the material. If material is not included in the article's Creative Commons licence and your intended use is not permitted by statutory regulation or exceeds the permitted use, you will need to obtain permission directly from the copyright holder. To view a copy of this licence, visit <http://creativecommons.org/licenses/by/4.0/>.

© The Author(s) 2022